AGU ADVANCING EARTH AND SPACE SCIENCE

Geophysical Research Letters

RESEARCH LETTER
10.1029/2020GL088627

Contributions of Greenland GPS Observed Deformation From Multisource Mass Loading Induced Seasonal and Transient Signals

Wenhao Li[1], C. K. Shum[2,3], Fei Li[1,4], Shengkai Zhang[1], Feng Ming[5], Wei Chen[3], Bao Zhang[6], Jintao Lei[7], and Qingchuan Zhang[1]

[1]Chinese Antarctic Center of Surveying and Mapping, Wuhan University, Wuhan, China, [2]Division of Geodetic Science, School of Earth Sciences, Ohio State University, Columbus, OH, USA, [3]Institute of Geodesy and Geophysics, Chinese Academy of Sciences, Wuhan, China, [4]State Key Laboratory of Information Engineering in Surveying Mapping and Remote Sensing, Wuhan University, Wuhan, China, [5]State Key Laboratory of Geo-information Engineering, Xi'an Institute of Surveying and Mapping, Xi'an, China, [6]School of Geodesy and Geomatics, Wuhan university, Wuhan, China, [7]Department of Land Surveying and Geo-Informatics, Hong Kong Polytechnic University, Hong Kong

Key Points:
- Interpretation of Greenland-wide 44 GPS deformation time series, manifested by multisource seasonal and transient mass loading signals
- We use M-SSA reconstructed Greenland GPS and modeled deformation data to quantify origins of spatiotemporal loading patterns
- Differenced GPS time series between adjacent sites reveals that locally varying seasonal signals are primarily attributable to SMB

Supporting Information:
- Supporting Information S1

Correspondence to:
F. Li,
fli@whu.edu.cn

Citation:
Li, W., Shum, C. K., Li, F., Zhang, S., Ming, F., Chen, W., et al. (2020). Contributions of Greenland GPS observed deformation from multisource mass loading induced seasonal and transient signals. *Geophysical Research Letters*, *47*, e2020GL088627. https://doi.org/10.1029/2020GL088627

Received 29 APR 2020
Accepted 1 JUL 2020
Accepted article online 8 JUL 2020

Abstract Global Positioning System (GPS) provides critical geodetic constraints on Earth's elastic response induced by ice and other mass loadings in Greenland. Previous studies focused on long-term ice mass changes, with relatively fewer studies on transient signals and had used fewer GPS stations. Here we reconstructed 44 Greenland-wide coastal decadal GPS time series using multichannel singular spectral analysis and quantified the origins of spatiotemporal patterns of transient to seasonal signals. We used an exhaustive list of geophysical processes, including surface mass balance (SMB), atmospheric pressure, continental hydrology, nontidal ocean loading, bedrock thermal expansion, precipitation, runoff, and ice discharge, and identified that most of Greenland's GPS sites exhibit SMB-induced transient signals during 2012–2015, with maximum displacement reaching 20.45 mm. Analyses of differenced time series between adjacent GPS stations near peripheral glaciers reveal that locally varying seasonal signals are primarily attributable to SMB, followed by atmosphere.

Plain Language Summary Prior studies on Greenland ice sheet mass change mainly focused on long-term and accelerated signals. However, the effects of multisource geophysical mechanisms on GPS observed transient or abrupt signals are relatively less studied, including quantifying locally varying spatiotemporal patterns between adjacent Global Positioning System (GPS) stations over entire Greenland. In this study, we model crustal displacements caused by an exhaustive list of geophysical mechanisms in Greenland, including atmospheric pressure, continental water storage, nontidal ocean circulation loading, bedrock thermal expansion, surface mass balance, and ice discharge. We then reconstruct the transient signals from 44 Greenland-wide coastal GPS decadal records using multichannel singular spectral analysis. The differenced time series between adjacent GPS stations located near the peripheral glaciers reveals that locally varying deformation is primarily caused by surface mass balance loading, followed by atmosphere loading. Most of GPS observed transient signals are attributable to surface mass balance and ice discharge loading, 2009 to mid-2011, and 2012 to 2015, which can reach a maximum displacement of 20.5 mm, with a mean displacement of 5.97 mm.

1. Introduction

Over the past decades, the rapid mass loss rate of the Greenland ice sheet (GrIS) has been exceeding that of Antarctica ice sheet under an increasingly warmer Earth. The global sea level would rise approximately 7 m if GrIS melts completely. The mass loss rate gradually increased from 2003 to summer of 2013, with extreme melting occurred in 2012, and 98% of the GrIS reached the melting temperature (Tedesco et al., 2013). After the summer of 2013, the melting suddenly stopped or nearly stopped for 12–18 months. Bevis et al. (2019) thought that the changes of ice mass loading are mostly driven by the air temperature and solar radiation and that continued atmospheric warming would lead to southwest Greenland being a major contributor to global sea level rise. The geophysical processes of ice mass loss rate are not steady. Surface mass balance (SMB), ice discharge (D), and calving front retreat have considerable effects on short-term changes of ice mass loss (Bondzio et al., 2017; Cassotto et al., 2015; Muresan et al., 2016; Zhang et al., 2018). SMB,

which is a crucial factor, is the difference of accumulation and ablation process. It has considerable annual and interannual characteristics (Abdalati & Steffen, 2001; Hanna et al., 2011). Previous studies have focused on long-term and annual changes (Kjeldsen et al., 2015; Khan et al., 2016; Liu et al., 2017; Shepherd et al., 2012) and the impact of short-term Greenland ice mass change on the estimation of long-term ice mass loss (Csatho et al., 2014; Ramillien et al., 2006; Velicogna, 2009; Velicogna & Wahr, 2006). However, relatively fewer studies are on the quantification of transient or abrupt geophysical processes induced GPS loading signals covering Greenland-wide coastal regions. In particular, transient signals originated from SMB and D would significantly affect short-term ice mass changes and, thus, impact long-term Greenland mass balance estimates. None of the studies listed above describe and explain the latest temporal and spatial short-term mass changes of GrIS. In particular, transient signals originated from SMB and D, by definition, vary with the climate cycle and would significantly affect short-term ice mass changes and, thus, impact long-term Greenland mass balance estimates. As the number of GPS sites and their observation records continue to increase, this research aims at systematically and thoroughly quantifying these present-day transient signals.

GPS is one of most important tools for studying mass changes in Greenland, via its sensitivity to the solid Earth's response to loading of ice mass change and other geophysical processes, and its accurate decadal or longer 3-D displacement time series. Since 2007, more than 50 stations have been built in Greenland to monitor the Earth's elastic and viscoelastic responses caused by ice mass change and other geophysical changes. For example, the transient changes of GrIS in 2012 have been observed (Khan et al., 2014, 2016; Nielsen et al., 2012, 2013). Zhang et al. (2017, 2018) applied multichannel singular spectral analysis (M-SSA) technique to estimate the transient mass changes near Greenland's Jakobshavn Isbræ glacier, the results showed that the anomalies in this area are mainly caused by glacier movement and SMB changes. Zhang et al. (2019) extracted transient mass changes of GrIS using 26 GPS stations; their results showed that the ice mass anomalies were caused by atmospheric circulation anomalies. With the increasing number of stations and data accumulation, the requirement of data accuracy also increases. Thus, quantitatively analyzing the temporal and spatial characteristics of annual signals and short-term transient signals and their effects on long-term is imperative.

GPS time series shows long-term trend and interannual variability. The long-term trend of Greenland GPS network (GNET) contains glacial isostatic adjustment signal over the past thousand years and elastic response caused by present-day variations on and near the GrIS (Khan et al., 2007, 2008, 2016). Annual variability is caused by surface mass loading, which is purely elastic and synchronous with the surface mass changes (Liu et al., 2017), including periodic movements caused by nontidal loading, such as ice mass loss, atmospheric pressure (ATM), continental hydrology (via the Global Land Data Assimilation System, or GLDAS model), and ocean circulation (via the Estimating the Circulation and Climate of the Ocean-2, or ECCO2 model). Wang et al. (2005) reported that the effects of geophysical factors on station position cannot be completely eliminated by harmonic analysis. Analysis and correction from the origin of geophysical processes are necessary. Therefore, the nontidal loading signals in GPS time series should be modeled and analyzed (Dong et al., 2002; Mao et al., 1999). Previous studies have focused on the annual variability of ice mass and the effect of atmospheric circulation (Bevis et al., 2012; Khan et al., 2016; Wahr et al., 2013). By contrast, other remaining geophysical loading signals in the GPS data and the locally varying geophysical signals between adjacent GPS stations located near ocean-flowing peripheral glaciers over the entire Greenland collectively lack quantitative analysis. Liu et al. (2017) explored the effects of nontidal loading and ice mass loading on the SRMP and UPVK stations to examine locally varying signals in the west coast of Greenland. Given the vast area of Greenland, the effects of nontidal loading and ice mass loading vary considerably in different regions. By analyzing the geophysical mechanisms of Greenland-wide coastal GPS vertical deformation in different drainage basins and covering the entire Greenland, we can effectively quantify the spatiotemporal the effects of different geophysical sources and detection of transient and seasonal signals in Greenland.

In this study, we investigate the seasonal and transient geophysical characteristics in the GPS data observed by 44 Greenland-wide GNET stations. The data sources considered include ATM, GLDAS, ECCO2, bedrock surface temperature (TEM), SMB, and D. First, we reconstruct and quantify the effects of SMB and D anomalies based on M-SSA. We then briefly describe the data sets used and the methodologies in section 2; each of geophysical deformation forward models or corrections is presented in section 3, followed by the study of identifying differential vertical displacements among adjacent stations, to assess Greenland-wide locally varying mass signals in section 4, and section 5 is the conclusions.

2. Methods and Data

2.1. GPS Data

The GPS time series records used in this study are download from Nevada Geodetic Laboratory, University of Nevada at Reno, corresponding to the IGb2008 data product. We select 44 GNET stations based on the integrity of GPS time series with the time span from 2008 to 2017. Here we adopt the Greenland basin convention by Rignot et al. (2011) and divided Greenland into six basins, namely, (1) north, (2) northeast, (3) southeast, (4) southwest, (5) central west, and (6) northwest (Figure S1 in the supporting information). Most of GPS stations are located adjacent to peripheral glaciers in coastal Greenland. Some offsetting effects occur in the horizontal direction. In this study, we focus on the vertical component. The average proportion of missing data of our time series is 13.28%. We use the third quartile criterion to remove outliers from the raw time series. To mitigate missing data in the time series, we use the regularized expectation–maximization (RegEM; Schneider, 2001) algorithm to interpolate and reconstruct the complete time series.

2.2. Loading Data

To determine the crustal deformation caused by more than ice mass loading, we calculate the contributions from other geophysical sources by modeling ATM, ECCO2, GLDAS, and TEM. The loading data of ATM, ECCO2, and GLDAS are from the School and Observatory of Earth Sciences Loading Service, University of Strasbourg. The ATM displacements are calculated using ECMWF reanalysis-5 data, ERA-5 (6 hr, 0.25°). The nontidal ocean loading is computed using the ECCO2 model output (daily, 0.25°). Continental hydrologic loading (primary snow and subglacial lakes) is estimated from GLDAS/Noah v1.0 model (3 hr, 0.25°). SMB loading is estimated using Regional Atmospheric Climate Model version 2.3 (RACMO 2.3; Noël et al., 2015, 2017; van Wessem et al., 2018). RACMO 2.3 provides SMB monthly solution data during 1958–2015 (11 km × 11 k m). We remove the 1961–1990 mean from the monthly fields and obtain the mass balance time series from 2008 to 2015. All loading data are resampled to match the GPS data. The ice discharge data (D) over Greenland have been studied by Bamber et al. (2018) and King et al. (2018). Here we used the data from Bamber et al. (2018) to calculate the crustal deformation at all the GPS locations. This data set updated and extended the original data set produced by Rignot et al. (2008), with new data which captured surface velocities at subannual temporal intervals for 195 outlet glaciers across Greenland. At each data grid, we use the Green's function to compute the elastic mass loading using the preliminary reference Earth model and the continental crust data to estimate the elastic response from the 3-D GPS displacements at each site (Dziewonski & Anderson, 1981; Jentzsch, 1997).

2.3. Bedrock Surface Temperature (TEM) Data

The change in surface temperature will transmit heat to the bedrock, which causes the temperature change of the bedrocks, inducing vertical deformation of all GPS stations in Greenland. The temperature data are from ERA-5 (daily sampling at 0.25° spatial resolution). According to Dong et al. (2002) and Yan et al. (2010), the vertical displacement of GPS station caused by surface temperature change can be obtained in the supporting information (Text S1).

2.4. Gravity Recovery and Climate Experiment (GRACE) Data

The University of Texas Center for Space Research GRACE RL06 data set is used this study. The monthly temporal gravity field is expressed in spherical harmonics or in Stokes coefficients, from April 2002 to June 2017. Data postprocessing steps include (1) replace the monthly low degree zonal coefficients, C_{20} and $C_{30,}$ with satellite laser ranging solutions (Loomis et al., 2019); (2) correction of Earth's ellipsoidal or oblateness effect (Li et al., 2017) to compute mass changes; (3) remove the GGM05 model (from January 2004 to December 2009) as the mean reference gravity field; (3) the ICE-6G-D forward model is chosen to correct for the glacial isostatic adjustment process (Peltier et al., 2018); (4) decorrelation and Gaussian filtering with a 300 km radius; (5) leakage corrections using the forward modeling method; and (6) we use the following formulae depicted by Equations 1–4 to compute the vertical displacement from the GRACE data:

$$\widehat{C}_{l_m}=\frac{1}{R}\cdot\frac{1}{4\pi}\iint_{\sigma} dh(\theta,\phi)\widetilde{P}_{l,\,m}(cos\ \theta)\cos(m\phi)d\sigma \tag{1}$$

$$\widehat{S}_{l_m}=\frac{1}{R}\cdot\frac{1}{4\pi}\iint_{\sigma} dh(\theta,\phi)\widetilde{P}_{l,\,m}(cos\ \theta)sin(m\phi)d\sigma \tag{2}$$

$$\begin{pmatrix} C_{l_m} \\ S_{l_m} \end{pmatrix} = \frac{3\rho_\omega}{\rho_{ave}} \frac{1+\kappa'_l}{2l+1} \begin{pmatrix} \widehat{C}_{l_m} \\ \widehat{S}_{l_m} \end{pmatrix} \quad (3)$$

Similar to Wahr et al. (1998), $\widehat{C}_{l_m}$ and $\widehat{S}_{l_m}$ are dimensionless Stokes coefficients; θ and ϕ are geocentric latitude and longitude, respectively; $d\sigma$ is the area element, which is same as $sin(\theta)d\theta d\varphi$; ρ_ω is density of water (1 g/cm^3), and ρ_{ave} is Earth's mean density (5.517 g/cm^3). Stokes coefficients C_{l_m} and S_{l_m} (Equation 3) are then used to calculate the vertical uplift (Equation 4), $dr(\theta, \phi)$ (van Dam et al., 2007):

$$dr(\theta,\phi) = R \sum_{l=0}^{\infty} \sum_{m=0}^{l} W_l \widetilde{P}_{l,m}(cos\ \theta)(C_{l_m}\cos(m\phi) + S_{l_m}\sin(m\phi)) \cdot \frac{h'_l}{1+\kappa'_l} \quad (4)$$

where R is the Earth's mean radius, $\widetilde{P}_{l,m}$ is the normalized Legendre function (l degree, m order), h'_l and κ'_l are the load Love numbers, and W_l is the weighting function (Jekeli, 1981; Wahr et al., 1998). We apply a Gaussian smoothing kernel of 300 km radius commensurate with the spatial resolution of GRACE data.

2.5. M-SSA

M-SSA is an improved SSA method (Chen et al., 2013; Ghil et al., 2002). It can effectively process multivariate data and has been successfully applied to GRACE data (Rangelova et al., 2010, 2012), GPS data (Walwer et al., 2016), and multivariate data set (Zhang et al., 2017). We briefly describe the theory in supporting information (Text S2), and further details can be obtained from Ghil et al. (2002) and Walwer et al. (2016).

3. Results

3.1. Nontidal Deformation

We first perform the spectral analysis for each of the GPS, ATM, ECCO2, GLDAS, TEM, SMB, and D time series. The result shows all of the time series are mainly affected by annual and semiannual variabilities. Thus, we consider the annual and semiannual periodicities in the least squares fitting. We calculate the crustal uplift caused by nontidal deformation on the basis of the above data and methods. The results of all stations are shown in Figures S2; GPS time series and all loading time series show obvious periodic characteristics. ATM has the maximum loading deformation, with maximum annual amplitude of 2.86 ± 1.7 mm (RINK station) and mean annual amplitude of 1.71 ± 0.64 mm. The deformation due to ECCO2 ocean circulation and GLDAS hydrologic loading is extremely small, resulting in changes of mean annual amplitudes to 0.36 ± 0.27 mm and 0.42 ± 0.11 mm, respectively. However, the ECCO2 and GLDAS loading deformation at the HEL2 station is considerably larger than its adjacent stations, resulting in changes of annual amplitudes of 1.17 ± 0.19 and 2.18 ± 1.32 mm, respectively. We interpret that the reason of the much larger loading signals at HEL2 is due primarily to its proximity at the entrance of Helheim glacier, where glacier activities and local weather conditions (such as sea breeze, atmospheric pressure change, and ocean heat exchange) are abundant.

3.2. Bedrock Temperature Change (TEM) Result

According to Equation 1, we calculate the uplift displacement caused by TEM at 44 GNET stations. The maximum change in temperature in Greenland can reach 15 °C, the maximum difference of vertical displacement caused by TEM is close to 3 mm, and the mean annual amplitude is 0.67 ± 0.16 mm. After removing TEM, annual amplitudes of 57% stations have been effectively reduced, and the maximum reduction is 47%. The variability of semiannual amplitudes is small. Thus, the thermal expansion effect mainly affects the annual variations of GPS time series but has little influence on the semi-annual term.

3.3. SMB Result

We calculate the uplift deformation caused by SMB using the RACMO 2.3 model. We also use GRACE data to calculate the elastic deformation induced displacements, sand compare them with SMB, and the annual amplitude difference between GRACE and SMB uplift deformation are presented in Figure S3**.** The stations are mainly distributed in the coastal areas of southeast Greenland, where GRACE data are shown to be consistent with those of SMB, especially at KULU, HJOR, and TIMM stations. The results are also consistent for other regions (Figure S4), which show that the mass change of these areas where the three stations are located are mainly caused by SMB. AASI, KMOR, and KULU stations having similar results. The

differences between GRACE and SMB are relatively large in other stations, and the SMB amplitudes are larger than GRACE. One reason can be the low resolution of GRACE. Conversely, other forms of mass change may still exist in Greenland, which offsets the SMB. KAGA station has the maximum uplift caused by SMB loading, with annual and semiannual amplitudes of 8.44 ± 2.02 and 1.65 ± 0.18 mm, respectively. Moreover, GROK, KELY, ILUL, SCBY, and BLAS have a large SMB deformation. The annual and semiannual amplitudes are larger than 5 and 1 mm, respectively. The stations with smaller amplitudes are mainly concentrated in the northeast and northwest coastal areas, and the annual amplitude is less than 1 mm.

3.4. Ice Discharge (D) Result

The mass changes and deformation caused by D are calculated in six subregions. Figure S5 is the mass changes of D, SMB, and GRACE, which shows that the mass changes caused by D is much smaller than SMB. We calculate the sum of the absolute values of D and SMB mass changes, and D is only 3.50%, 2.19%, 4.15%, 2.79%, 1.38%, and 4.91% of SMB in six subbasins in Greenland. Furthermore, we calculate the displacement caused by D (Figure S6); the maximum displacement appears in NW (3.27 mm, TIMM); however, the corresponding GPS displacement is 46.74 mm. In other regions, the displacement is no more than 1 mm. Therefore, we conclude that the crustal deformation caused by D has no significant effect on the GPS uplift.

3.5. Applying Geophysical Corrections to GPS

Table S1 presents the amplitudes of GPS, ATM, ECCO2, GLDAS, SMB, and TEM. The maximum annual amplitude of GPS is 7.04 ± 4.61 mm (SENU), and the mean amplitude is 3.22 ± 1.49 mm. SMB has the maximum influence, with a mean annual amplitude of 2.32 ± 0.91 mm. ATM has the second largest influence, with a mean annual amplitude of 1.71 ± 0.64 mm. Southern Greenland is larger than the northern Greenland. ECCO2, GLDAS, and TME have the least influence, with mean annual amplitudes of 0.36 ± 0.27, 0.42 ± 0.11, and 0.67 ± 0.16 mm, respectively; considering the displacement caused by D is very small, the results are not considered in this section and in section 4.1.

Table S3 lists the amplitude varieties of GPS time series before and after removing each correction. The mean reduction of annual amplitude is 0.96 ± 0.41, 0.19 ± 0.11, 0.11 ± 0.05, and 0.18 ± 0.08 mm after removing the ATM, ECCO2, GLDAS, and TEM, respectively. After removing the four corrections, the reduction of maximum and mean annual amplitude is 2.8 ± 0.54 and 1.08 ± 0.36 mm, respectively. However, after removing SMB, the annual amplitude becomes large in some stations; the semiannual amplitude has small changes, which show the GPS uplift deformation caused by SMB mainly affects the annual variations. Moreover, the phase has changed considerably before and after removing SMB in the stations with increased amplitude, and the phase change is small in stations with reduced amplitude. Thus, other factors in the stations have important contributions to the vertical seasonal variations of the Earth's surface; these factors include the seasonal error of atmospheric model in tropospheric refraction correction, phase center model error and multipath effect, the influence of software and solution strategy, and the influence of reference frame offsets (Dong et al., 2002).

4. Discussions

4.1. Differential Vertical Displacements Among Adjacent Stations

After removing all the corrections, periodic terms still exist in some stations, particularly those mainly concentrated in stations close to and far away from glaciers, which we infer may be caused by SMB differences. Some stations are selected for analysis to determine the mechanism of periodic terms in GPS time series. Figure S7a shows the distribution of DGJG, SCOR, and VEDG and the difference of GPS and all correction time series. Figure S7b shows the differential time series (DTS) of DGJG and SCOR. We can see the differences are caused by SMB and ATM. We initially remove the ATM of DGJG and SCOR. The annual amplitude of DTS decreases from 1.21 ± 0.46 to 0.97 ± 0.24 mm. After further removing the ECCO2, GLDAS, and TEM, the annual amplitude drops to 0.69 ± 0.34 mm. Finally, after removing SMB, the annual amplitude drops to 0.34 ± 0.49 mm. The semiannual amplitude changes significantly after removing ATM, from 0.74 ± 0.26 to 0.38 ± 0.22 mm. After further removing other corrections, the semiannual amplitude remains unchanged. Similar results occur between VFDG and SCOR. The effects of all corrections are similar in DGJG and SCOR. The annual amplitude of the DTS between DGJG and SCOR is nearly zero.

We conduct the same analyses for KAGA, IULU, and AASI. The DTS of SMB and GPS are highly correlated (Figures S8b and S8c). We initially remove the four corrections (except SMB). The DTS of KAGA and IULU have small changes (3.36 ± 2.03 to 3.24 ± 1.87 mm). After further removing SMB, the annual amplitude decreases to 2.12 mm. For KAGA and AASI, the annual amplitude changes from 4.56 ± 2.28 to 4.64 ± 1.95 mm and then to 1.62 ± 0.74 mm after removing the four corrections and SMB. KAGA and IULU are near the Sermeq Kujalleq glacier and are affected greatly by glacier movement. Although IULU is far away from GrIS, the difference between IULU and AASI is mainly caused by SMB. We also calculate the SMB effect between IULU and AASI. After removing SMB, the annual amplitude of DTS decreases from 2.41 ± 0.11 to 1.05 ± 0.59 mm.

We also analyze the DTS of NNVA, QAQ1, and SENU, and the results are similar to the two aforementioned areas (Figure S9). The SMB difference among the three stations is small, because QAQ1 station is close to GrIS. The rest of the corrections have relatively smaller effects. The detailed results list in Table S5. The difference among GPS stations near the GrIS is mainly caused by SMB, followed by ATM.

4.2. Transient Signals Caused by SMB and D

We find that the GPS and SMB time series have evident uplifts in some stations during 2012–2015. Zhang et al. (2017) found that the uplifts are caused by SMB for a few GPS stations. To further extract the transient signals and quantify the influence of SMB-induced transient signals over entire Greenland, we apply M-SSA (Rangelova et al., 2010, 2012; Walwer et al., 2016) to GPS and GRACE data. The choice of M-SSA window width M is a trade-off between the quantity of extracted information and the statistical confidence of the extracted modes. Larger N/M (N is the length of data) ratio gives better results (Ghil et al., 2002). We follow the approach in Zhang et al. (2017) to apply M-SSA with a window width of 700 days to the time series. We adopt the MC-SSA (Allen & Robertson, 1996; Allen & Smith, 1996) to confirm the number of significant PCs (Text S3). Meanwhile, we take the spatial correlation of geophysical signals into account to further distinguish the transient signals and use the eigenvalues to represent the variance of transient signals, where the percentage of variance is the signal strength.

We use GPS and GRACE data to formulate a two-channel SSA and SMB to one-channel SSA. Given the much coarser resolution of GRACE at 333 km half wavelength, the displacement derived from GRACE is much smaller than GPS, which represents a point value. We follow Khan et al. (2010) approach to apply scale factors to the GRACE-computed vertical displacements at each of the GPS sites, which allows better comparisons between GRACE and GPS observations. Then, we reconstruct the transient signals of NRSK station (Figure 1a). The transient signals of GPS, GRACE, and SMB are highly consistent and showed signal increases during 2012–2013 and decreases during 2013–2015, which reveal that the transient signal is caused by SMB. We perform M-SSA for all 44 stations in Greenland and find that 42 stations have transient signals similar to NRSK during 2012–2015 (Figure S10). Thus, GPS stations in Greenland are generally affected by SMB transient signal during this time period. We use peak-to-peak values to quantify the transient variations. The maximum displacements of GPS time series caused by SMB transient signal is presented in Figure 1b, with more detailed information listed in Table S6. The maximum displacement of GPS time series caused by SMB transient signal is approximately 20.54 mm, and the mean displacement is 5.97 mm. The southwest of Greenland (subregion 3) is the most affected area, and the stations close to the GrIS and glaciers are more affected than those along the coast.

We find that GPS and GRACE also have a reduction of the transient signal in 2011, whereas SMB does not. Zhang et al. (2017, 2019) confirmed that the transient signals are caused by D. To quantify the effect of D anomalies and patterns, we calculate the anomalies in all stations and find the anomalies show a very similar varying trend with the GPS transient signals during 2009 and 2011 (such as TIMM shown in Figure S11). The D shows a gentle subsidence from 2009 to mid-2011, which exhibits similar temporal patterns as in the GPS, though with a smaller amplitude. This trend is also found in many SMB transient signals (such as MIK2, NNVN, QAQ1 etc.). This suggests that the anomalies during this period were due to the combined contributions from both D (ice discharges) and SMB. We use M-SSA to reconstruct the D anomalies in Figure 1c, which shows that the maximum anomaly appears only in NW (SRMP and UPVK), and they are close to 3 mm. However, D anomalies have much smaller effects on crustal displacement in other regions.

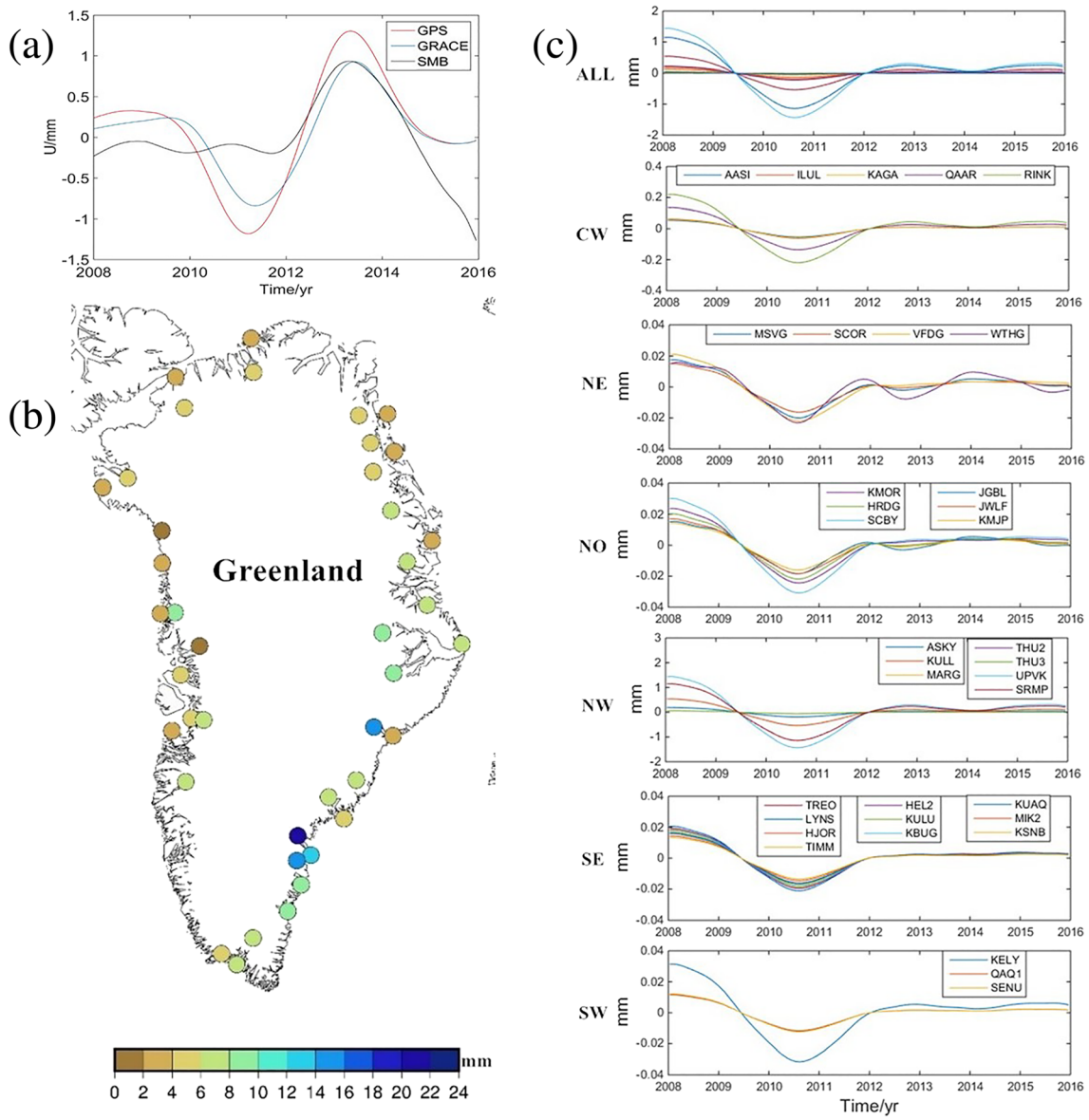

Figure 1. (a) The reconstructed transient signals at the NRSK station (red line is GPS, blue line is GRACE, and gray line is SMB time series, respectively); (b) the magnitude maximum displacements of GPS time series caused by transient SMB; (c) the transient signals caused by ice discharge.

In Greenland, dynamic ice mass redistribution also accounts for a large portion of ice dynamics. Here to determine the main contribution to the GPS transient signals, we perform the sensitivity of loading contributions using SMB data (Figure S12), which shows that the bedrock's measured displacement decreases very quickly with increasing distance from the source. In addition, the inland dynamic ice mass redistribution may contribute very little to the GPS transient displacements since the GPS sites were deployed on the coastal bedrocks near the coast. Zhang et al. (2017, 2018) have reconstructed the transient signals using SMB + D (or ice discharges) in the Upernavik and Jakobshavn glaciers. In both cases, it is revealed that the transient displacements modeled by SMB + D agree very well with the transient signal extracted from GPS bedrock time series and that the most transient motions are attributable to SMB + D.

4.3. The Spatial Characteristics of SMB and GPS Displacements

We remove the trend for all the time series and compare the time series for both GPS, SMB uplifts, and SMB, GRACE mass changes (Figure 2, left). All of them reveal strong similarities in amplitudes and phases. From Figure 2 (left), we can find that SMB is the main contribution for Greenland mass changes, especially in SE;

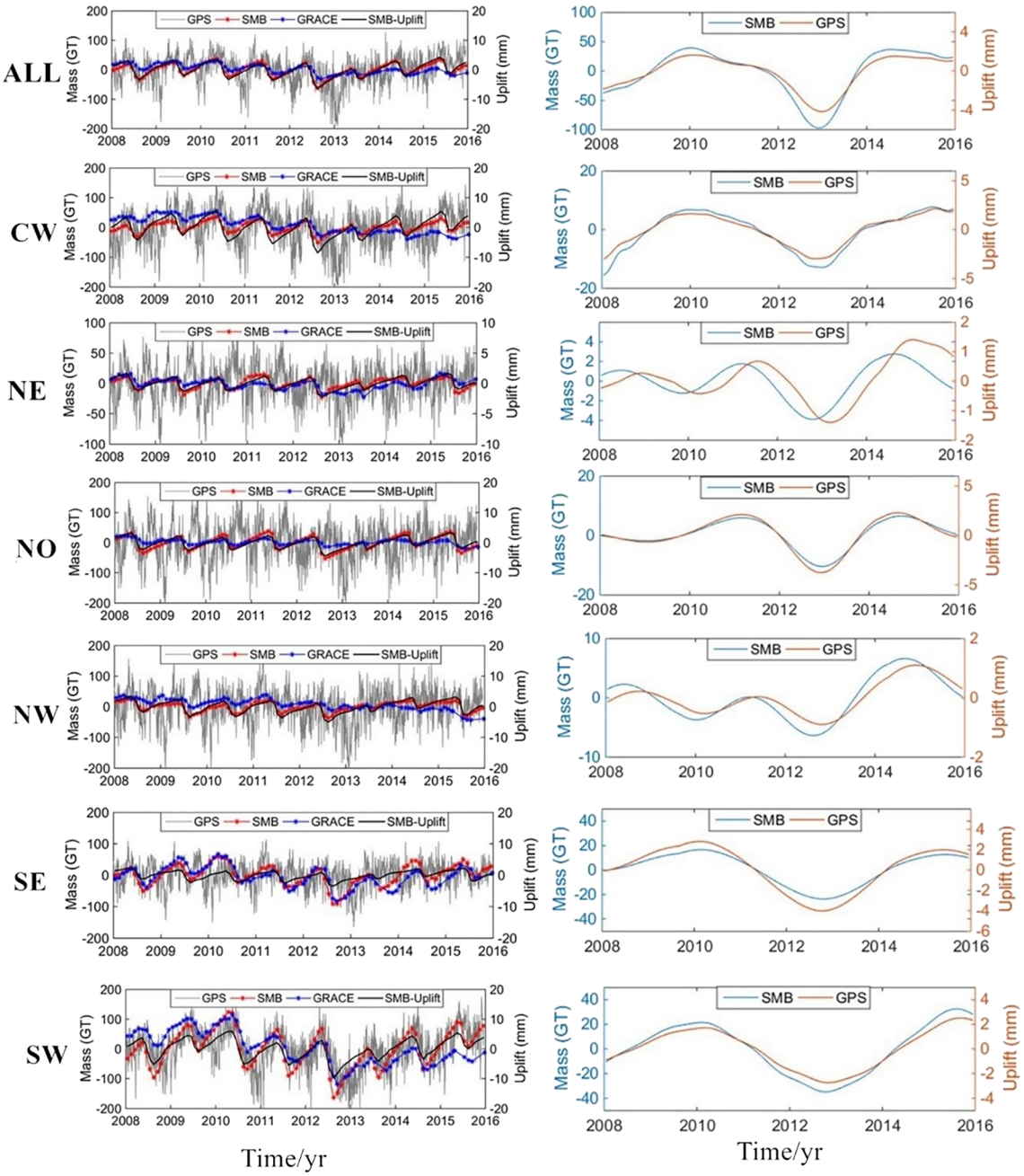

Figure 2. The uplift time series of GPS and SMB, the corresponding mass changes time series of SMB and GRACE in Greenland, each of the six subregions (left panel), and the variations of transient signals from SMB and GPS: 2008–2016 (right panel).

the correlation between SMB and GRACE mass changes is 90.2%; the amplitude and phase are very similar, and this means the mass loading displacements are mainly caused by SMB in SE. We reconstruct the seasonal signals for the time series of GPS uplift, SMB uplift, SMB mass, and GRACE mass in every subregion, which also has strong similarities (Figure S13).

Figure 2 (right) is the variations of transient signals of SMB and GPS, the results list in Table S7. The mass change in every subregion have similar patterns as GPS, but their amplitudes (peak to peak) are different. SE and SW have the largest amplitudes (40.37 and 56.48 Gt, respectively), and CW and NO have relatively smaller amplitudes (10.70 and 16.42 Gt, respectively). However, NE and NW have different patterns, with sustained mass loss from 2008 to 2010, then with sustained mass gain from 2010 to 2013; however, the

amplitude is only 1.70 and 0.87 Gt, respectively. Considering the low signal to noise in these regions, the signal may not be real, and we decided not to conduct further investigations.

Furthermore, due to runoff and precipitation are the two most important components to SMB in Greenland, we quantify the contribution both of them in every subregion (Figure S14); we can conclude that the SMB is mainly affected by runoff from both entire and local perspective, and runoff have the largest effect in SW. We also calculate the transient signals by runoff and precipitation (Figure S15); we can see that the effect of precipitation anomalies is quite small, and SMB anomalies are mainly caused by runoff. The pattern of runoff anomalies in CW, NO, SE, and SW Greenland regions is consistent with SMB but with poor agreements in NE and NW Greenland. It is noteworthy that precipitation have the similar pattern with SMB in SE; we compare the anomalies of GPS with SMB, runoff, and precipitation during 2011 to 2013 in Figure S16; we find that SE Greenland has the largest precipitation, which significantly affected SMB. Therefore, precipitation is also an important contribution to SMB anomalies in SE Greenland. The spatial characteristics of anomalies in the South are larger than in North from the entire Greenland perspective, and SE has the largest anomalies, indicating more ice mass loss.

5. Conclusions

In this study, we modeled crustal displacements caused by ATM, GLDAS, ECCO2, TEM, SMB, and D for 44 Greenland-wide GNET stations. We quantify the effect of each geophysical mechanism from the entire and local perspectives of Greenland on the GPS time series. Finally, we reconstruct transient signals caused by SMB and D based on M-SSA. Our findings and conclusions are as follows.

1. Throughout Greenland, SMB has the maximum influence on the loading signals in the GPS time series. Next is ATM, while ECCO2, GLDAS, and TEM processes have the least influence. From the local perspective, the differences of adjacent GPS stations near the glacier area are mainly caused by SMB, followed by ATM. The loading effects of other processes and from TEM are relatively small.
2. SMB anomalies are mainly caused by runoff, most of GPS stations are generally affected by SMB transient signals in 2012–2015. Subsidence anomalies during 2009 to mid-2011 were due primarily to the combined contributions from both SMB and D.

Conflicts of Interest

The authors declare that there is no conflict of interest.

Data Availability Statement

The GPS velocity data used in this study are available at: http://geodesy.unr.edu/NGLStationPages/GlobalStationList; the loading data of ATM, ECCO2, and GLDAS are from the School and Observatory of Earth Sciences Loading Service, University of Strasbourg: http://loading.u-strasbg.fr/displ_all.php; the ERA-5 temperature reanalysis data set is from https://cds.climate.copernicus.eu; the NASA/DLR GRACE data product is from http://icgem.gfz-potsdam.de/series; the RACMO SMB data set is from https://www.projects.science.uu.nl/iceclimate/models/racmo.php; the Greenland ice discharge data set is from https://www.bodc.ac.uk/data/published_data_library/catalogue/10.5285/643aa9bc-bcd6-45ad-e053-6c86abc07da0/ website.

Acknowledgments

The numerical calculations in this paper were conducted in the Supercomputing Center of Wuhan University. We acknowledge scientific data providers for their data sets used in this study. We thank Yan Jiang, Natural Resources Canada, and an anonymous reviewer for providing constructive comments, which have improved this manuscript. This research was supported by the National Key Research and Development Program of China (2017YFA0603104, 017YFA0603103), the State Key Program of National Natural Science Foundation of China (41531069, 41974040), and by the Strategic Priority Research Program of the Chinese Academy of Sciences (XDA19070302).

References

Abdalati, W., & Steffen, K. (2001). Greenland ice sheet melt extent: 1979–1999. *Journal of Geophysical Research*, *106*, 33,983–33,988. https://doi.org/10.1029/2001JD900181

Allen, M. R., & Robertson, A. W. (1996). Distinguishing modulated oscillations from coloured noise in multivariate datasets. *Climate Dynamics*, *12*(11), 775–784. https://doi.org/10.1007/s003820050142

Allen, M. R., & Smith, L. A. (1996). Monte Carlo SSA: Detecting irregular oscillations in the presence of colored noise. *Journal of Climate*, *9*(12), 3373–3404. https://doi.org/10.1175/1520-0442

Bamber, J. L., Tedstone, A. J., King, M. D., Howat, I. M., Enderlin, E. M., van den Broeke, M. R., & Noel, B. (2018). Land ice freshwater budget of the Arctic and North Atlantic Oceans: 1. Data, methods, and results. *Journal of Geophysical Research: Oceans*, *123*, 1827–1837. https://doi.org/10.1002/2017JC013605

Bevis, M., Harig, C., Khan, S. A., Brown, A., Simons, F. J., Willis, M., et al. (2019). Accelerating changes in ice mass within Greenland, and the ice sheet's sensitivity to atmospheric forcing. *Proceedings of the National Academy of Sciences of the United States of America*, *116*(6), 1934–1939. https://doi.org/10.1073/pnas.1806562116

Bevis, M., Wahr, J., Khan, S. A., Madsen, F. B., Brown, A., Willis, M., et al. (2012). Bedrock displacements in Greenland manifest ice mass variations, climate cycles and climate change. *Proceedings of the National Academy of Sciences of the United States of America*, *109*(30), 11944–11948. https://doi.org/10.1073/pnas.1204664109

Bondzio, J. H., Morlighem, M., Seroussi, H., Kleiner, T., Ruckamp, M., Mouginot, J., et al. (2017). The mechanisms behind Jakobshavn Isbrae's acceleration and mass loss: A 3-D thermomechanical model study. *Geophysical Research Letters*, *44*, 6252–6260. https://doi.org/10.1002/2017GL073309

Cassotto, R., Fahnestock, M., Amundson, J. M., Truffer, M., & Joughin, I. (2015). Seasonal and interannual variations in ice melange and its impact on terminus stability, Jakobshavn Isbrae, Greenland. *Journal of Glaciology*, *61*(225), 76–88. https://doi.org/10.3189/2015JoG13J235

Chen, Q., van Dam, T., Sneeuw, N., Collilieux, X., Weigelt, M., & Rebischung, P. (2013). Singular spectrum analysis for modeling seasonal signals from GPS time series. *Journal of Geodynamics*, *72*, 25–35. https://doi.org/10.1016/j.jog.2013.05.005

Csatho, B. M., Schenk, A. F., van der Veen, C. J., Babonis, G., Duncan, K., Rezvanbehbahani, S., et al. (2014). Laser altimetry reveals complex pattern of Greenland Ice Sheet dynamics. *Proceedings of the National Academy of Sciences of the United States of America*, *111*(52), 18,478–18,483. https://doi.org/10.1073/pnas.1411680112

Dong, D., Fang, P., Bock, Y., Cheng, M. K., & Miyazaki, S. (2002). Anatomy of apparent seasonal variations from GPS-derived site position time series. *Journal Of Geophysical Research*, *107*(B4). https://doi.org/10.1029/2001JB000573

Dziewonski, A., & Anderson, D. (1981). Preliminary Reference Earth Model (PREM). *Physics of the Earth and Planetary Interiors*, *25*(4), 297–356. https://doi.org/10.1016/0031-9201(81)90046-7

Ghil, M., Allen, M. R., Dettinger, M. D., Ide, K., Kondrashov, D., Mann, M. E., et al. (2002). Advanced spectral methods for climatic time series. *Reviews of Geophysics*, *40*(1), 1003. https://doi.org/10.1029/2000rg000092

Hanna, E., Huybrechts, P., Cappelen, J., Steffen, K., Bales, R. C., Burgess, E., et al. (2011). Greenland Ice Sheet surface mass balance 1870 to 2010 based on twentieth century reanalysis, and links with global climate forcing. *Journal of Geophysical Research*, *116*(D24), D24121. https://doi.org/10.1029/2011JD016387

Jekeli, C. (1981). Modifying stokes function to reduce the error of geoid undulation computations. *Journal of Geophysical Research*, *86*(B8), 6985–6990. https://doi.org/10.1029/JB086ib08p06985

Jentzsch, G. (1997). Earth tides and ocean tidal loading. In H. Wilhelm, W. Zurn, & H. G. Wenzel (Eds.), *Tidal Phenomena* (pp. 145–171). Berlin: Springer. https://doi.org/10.1007/BFb0011461

Khan, S. A., Kjaer, K. H., Bevis, M., Bamber, J. L., Wahr, J., Kjeldsen, K. K., et al. (2014). Sustained mass loss of the northeast Greenland ice sheet triggered by regional warming. *Nature Climate Change*, *4*(4), 292–299. https://doi.org/10.1038/Nclimate2161

Khan, S. A., Liu, L., Wahr, J., Howat, I., Joughin, I., van Dam, T., & Fleming, K. (2010). GPS measurements of crustal uplift near Jakobshavn Isbræ due to glacial ice mass loss. *Journal of Geophysical Research*, *115*, B09405. https://doi.org/10.1029/2010JB007490

Khan, S. A., Sasgen, I., Bevis, M., van Dam, T., Bamber, J. L., Wahr, J., et al. (2016). Geodetic measurements reveal similarities between post-Last Glacial Maximum and present-day mass loss from the Greenland Ice Sheet. *Science Advances*, *2*(9), e1600931. https://doi.org/10.1126/sciadv.1600931

Khan, S. A., Wahr, J., Leuliette, E., van Dam, T., Larson, K. M., & Francis, O. (2008). Geodetic measurements of postglacial adjustments in Greenland. *Journal Of Geophysical Research*, *113*(B2), B02402. https://doi.org/10.1029/2007JB004956

Khan, S. A., Wahr, J., Stearns, L. A., Hamilton, G. S., van Dam, T., Larson, K. M., & Francis, O. (2007). Elastic uplift in southeast Greenland due to rapid ice mass loss. *Geophysical Research Letters*, *34*, L21701. https://doi.org/10.1029/2007gl031468

King, M., Howat, I., Jeong, S., Noh, M.-J., Wouters, B., Noël, B., et al. (2018). Seasonal to decadal variability in ice discharge from the Greenland Ice Sheet. *The Cryosphere Discussions*, *12*(12), 3813–3825. https://doi.org/10.5194/tc-12s3813-2018

Kjeldsen, K. K., Korsgaard, N. J., Bjork, A. A., Khan, S. A., Box, J. E., Funder, S., et al. (2015). Spatial and temporal distribution of mass loss from the Greenland Ice Sheet since AD 1900. *Nature*, *528*(7582), 396–400. https://doi.org/10.1038/nature16183

Li, J., Chen, J. L., Li, Z., Wang, S. Y., & Hu, X. G. (2017). Ellipsoidal correction in GRACE surface mass change estimation. *Journal Of Geophysical Research: Solid Earth*, *122*, 9437–9460. https://doi.org/10.1002/2017JB014033

Liu, L., Khan, S. A., van Dam, T., Ma, J. H. Y., & Bevis, M. (2017). Annual variations in GPS-measured vertical displacements near Upernavik Isstrom (Greenland) and contributions from surface mass loading. *Journal Of Geophysical Research: Solid Earth*, *122*, 677–691. https://doi.org/10.1002/2016JB013494

Loomis, B. D., Luthcke, S. B., & Sabaka, T. J. (2019). Regularization and error characterization of GRACE mascons. *Journal of Geodesy*, *93*(9), 1399–1399. https://doi.org/10.1007/s00190-019-01286-2

Mao, A. L., Harrison, C. G. A., & Dixon, T. H. (1999). Noise in GPS coordinate time series. *Journal Of Geophysical Research*, *104*(B2), 2797–2816. https://doi.org/10.1029/1998JB900033

Muresan, I. S., Khan, S. A., Aschwanden, A., Khroulev, C., Van Dam, T., Bamber, J., et al. (2016). Modelled glacier dynamics over the last quarter of a century at Jakobshavn Isbrae. *The Cryosphere*, *10*(2), 597–611. https://doi.org/10.5194/tc-10-597-2016

Nielsen, K., Khan, S. A., Korsgaard, N. J., Kjaer, K. H., Wahr, J., Bevis, M., et al. (2012). Crustal uplift due to ice mass variability on Upernavik Isstrom, West Greenland. *Earth and Planetary Science Letters*, *353-354*, 182–189. https://doi.org/10.1016/j.epsl.2012.08.024

Nielsen, K., Khan, S. A., Spada, G., Wahr, J., Bevis, M., Liu, L., & van Dam, T. (2013). Vertical and horizontal surface displacements near Jakobshavn Isbrae driven by melt-induced and dynamic ice loss. *Journal Of Geophysical Research: Solid Earth*, *118*, 1837–1844. https://doi.org/10.1002/jgrb.50145

Noël, B., van de Berg, W. J., van Meijgaard, E., Kuipers Munneke, P., van de Wal, R. S. W., & van den Broeke, M. R. (2015). Evaluation of the updated regional climate model RACMO2.3: Summer snowfall impact on the Greenland Ice Sheet. *The Cryosphere*, *9*(5), 1831–1844. https://doi.org/10.5194/tc-9-1831-2015

Noël, B., van de Berg, W. J., van Wessem, J. M., van Meijgaard, E., van As, D., Lenaerts, J. T., et al. (2017). Modelling the climate and surface mass balance of polar ice sheets using RACMO2, Part 1: Greenland (1958-2016). *The Cryosphere*, *12*(3), 811–831. https://doi.org/10.5194/tc-12-811-2018

Peltier, W. R., Argus, D. F., & Drummond, R. (2018). Comment on "An assessment of the ICE-6G_C (VM5a) Glacial Isostatic Adjustment Model", by Purcell et al. *Journal Of Geophysical Research: Solid Earth*, *123*, 2019–2028. https://doi.org/10.1002/2016JB013844

Ramillien, G., Lombard, A., Cazenave, A., Ivins, E. R., Llubes, M., Remy, F., & Biancale, R. (2006). Interannual variations of the mass balance of the Antarctica and Greenland ice sheets from GRACE. *Global and Planetary Change*, *53*(3), 198–208. https://doi.org/10.1016/j.gloplacha.2006.06.003

Rangelova, E., Sideris, M. G., & Kim, J. W. (2012). On the capabilities of the multi-channel singular spectrum method for extracting the main periodic and non-periodic variability from weekly GRACE data. *Journal of Geodynamics*, *54*, 64–78. https://doi.org/10.1016/j.jog.2011.10.006

Rangelova, E., van der Wal, W., Sideris, M. G., & Wu, P. (2010). Spatiotemporal analysis of the GRACE-derived mass variations in North America by means of multi-channel singular spectrum analysis. *Gravity, Geoid And Earth Observation*, *135*, 539–546. https://doi.org/10.1007/978-3-642-10634-7_72

Rignot, E., Box, J. E., Burgess, E., & Hanna, E. (2008). Mass balance of the Greenland Ice Sheet from 1958 to 2007. *Geophysical Research Letters*, *35*, L20502. https://doi.org/10.1029/2008GL035417

Rignot, E., Velicogna, I., van den Broeke, M. R., Monaghan, A., & Lenaerts, J. (2011). Acceleration of the contribution of the Greenland and Antarctic ice sheets to sea level rise. *Geophysical Research Letters*, *38*, L05503. https://doi.org/10.1029/2011gl046583

Schneider, T. (2001). Analysis of incomplete climate data: Estimation of mean values and covariance matrices and imputation of missing values. *Journal of Climate*, *14*(5), 853–871. https://doi.org/10.1175/1520-0442(2001)014<0853:Aoicde>2.0.Co;2

Shepherd, A., Ivins, E. R., Geruo, A., Barletta, V. R., Bentley, M. J., Bettadpur, S., et al. (2012). A reconciled estimate of ice-sheet mass balance. *Science*, *338*(6111), 1183–1189. https://doi.org/10.1126/science.1228102

Tedesco, M., Fettweis, X., Mote, T., Wahr, J., Alexander, P., Box, J. E., & Wouters, B. (2013). Evidence and analysis of 2012 Greenland records from spaceborne observations, a regional climate model and reanalysis data. *The Cryosphere*, *7*(2), 615–630. https://doi.org/10.5194/tc-7-615-2013

van Dam, T., Wahr, J., & Lavallee, D. (2007). A comparison of annual vertical crustal displacements from GPS and Gravity Recovery And Climate Experiment (GRACE) over Europe. *Journal Of Geophysical Research*, *112*, B03404. https://doi.org/10.1029/2006JB004335

Van Wessem, J. M., van de Berg, W. J., Noël, B. P. Y., van Meijgaard, E., Amory, C., Birnbaum, G., et al. (2018). Modelling the climate and surface mass balance of polar ice sheets using RACMO2, Part 2: Antarctica (1979–2016). *The Cryosphere*, *12*(4), 1479–1498. https://doi.org/10.5194/tc-12-1479-2018

Velicogna, I. (2009). Increasing rates of ice mass loss from the Greenland and Antarctic ice sheets revealed by GRACE. *Geophysical Research Letters*, *36*, L19503. https://doi.org/10.1029/2009GL040222

Velicogna, I., & Wahr, J. (2006). Acceleration of Greenland ice mass loss in spring 2004. *Nature*, *443*(7109), 329–331. https://doi.org/10.1038/nature05168

Wahr, J., Khan, S. A., van Dam, T., Liu, L., van Angelen, J. H., van den Broeke, M. R., & Meertens, C. M. (2013). The use of GPS horizontals for loading studies, with applications to northern California and southeast Greenland. *Journal Of Geophysical Research: Solid Earth*, *118*, 1795–1806. https://doi.org/10.1002/jgrb.50104

Wahr, J., Molenaar, M., & Bryan, F. (1998). Time variability of the Earth's gravity field: Hydrological and oceanic effects and their possible detection using GRACE. *Journal Of Geophysical Research*, *103*(B12), 30,205–30,229. https://doi.org/10.1029/98JB02844

Walwer, D., Calais, E., & Ghil, M. (2016). Data-adaptive detection of transient deformation in geodetic networks. *Journal Of Geophysical Research: Solid Earth*, *121*, 2129–2152. https://doi.org/10.1002/2015JB012424

Wang, M., Shen, Z. K., & Dong, D. N. (2005). Effects of non-tectonic crustal deformation on continuous GPS position time series and correction to them. *Chinese Journal Of Geophysics-Chinese Edition*, *48*(5), 1121–1129. https://doi.org/10.1002/cjg2.755

Yan, H. M., Chen, W., Zhu, Y. Z., Zhang, W. M., Zhong, M., & Liu, G. Y. (2010). Thermal effects on vertical displacement of GPS stations in China. *Chinese Journal Of Geophysics-Chinese Edition*, *53*(4), 825–832. https://doi.org/10.3969/j.issn.0001-5733.2010.04.007

Zhang, B., Liu, L., Khan, S. A., van Dam, T., Bjork, A. A., Peings, Y., et al. (2019). Geodetic and model data reveal different spatio-temporal patterns of transient mass changes over Greenland from 2007 to 2017. *Earth and Planetary Science Letters*, *515*, 154–163. https://doi.org/10.1016/j.epsl.2019.03.028

Zhang, B., Liu, L., Khan, S. A., van Dam, T., Zhang, E. Z., & Yao, Y. B. (2017). Transient variations in glacial mass near Upernavik Isstrom (West Greenland) detected by the combined use of GPS and GRACE data. *Journal Of Geophysical Research: Solid Earth*, *122*, 10,626–10,642. https://doi.org/10.1002/2017JB014529

Zhang, B., Zhang, E. Z., Liu, L., Khan, S. A., van Dam, T., Yao, Y. B., et al. (2018). Geodetic measurements reveal short-term changes of glacial mass near Jakobshavn Isbrae (Greenland) from 2007 to 2017. *Earth and Planetary Science Letters*, *503*, 216–226. https://doi.org/10.1016/j.epsl.2018.09.029